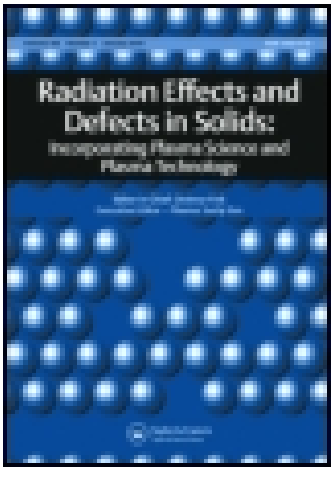

Radiation Effects and Defects in Solids: Incorporating Plasma Science and Plasma Technology
Publication details, including instructions for authors and subscription information:
http://www.tandfonline.com/loi/grad20

SEM and Raman spectroscopy analyses of laser-induced periodic surface structures grown by ethanol-assisted femtosecond laser ablation of chromium

Shazia Bashir[ab], M. Shahid Rafique[ac], Chandra S.R. Nathala[a], Ali Ajami[a] & Wolfgang Husinsky[a]

[a] Institute of Applied Physics, Vienna University of Technology, Vienna, Austria

[b] Centre for Advanced Studies in Physics, GC University Lahore, Lahore, Pakistan

[c] Department of Physics, University of Engineering and Technology Lahore, Lahore, Pakistan

Published online: 01 Apr 2015.

To cite this article: Shazia Bashir, M. Shahid Rafique, Chandra S.R. Nathala, Ali Ajami & Wolfgang Husinsky (2015): SEM and Raman spectroscopy analyses of laser-induced periodic surface structures grown by ethanol-assisted femtosecond laser ablation of chromium, Radiation Effects and Defects in Solids: Incorporating Plasma Science and Plasma Technology, DOI: 10.1080/10420150.2015.1023202

To link to this article: http://dx.doi.org/10.1080/10420150.2015.1023202

Radiation Effects & Defects in Solids, 2015
http://dx.doi.org/10.1080/10420150.2015.1023202

SEM and Raman spectroscopy analyses of laser-induced periodic surface structures grown by ethanol-assisted femtosecond laser ablation of chromium

Shazia Bashir[a,b*], M. Shahid Rafique[a,c], Chandra S.R. Nathala[a], Ali Ajami[a], and Wolfgang Husinsky[a]

[a]*Institute of Applied Physics, Vienna University of Technology, Vienna, Austria;* [b]*Centre for Advanced Studies in Physics, GC University Lahore, Lahore, Pakistan;* [c]*Department of Physics, University of Engineering and Technology Lahore, Lahore, Pakistan*

(*Received 2 September 2014; accepted 17 February 2015*)

The effect of fluence and pulse duration on the growth of nanostructures on chromium (Cr) surfaces has been investigated upon irradiation of femtosecond (fs) laser pulses in a liquid confined environment of ethanol. In order to explore the effect of fluence, targets were exposed to 1000 pulses at various peak fluences ranging from 4.7 to 11.8 J cm^{-2} for pulse duration of $\sim$25 fs. In order to explore the effect of pulse duration, targets were exposed to fs laser pulses of various pulse durations ranging from 25 to 100 fs, for a constant fluence of 11.8 J cm^{-2}. Surface morphology and structural transformations have been analyzed by scanning electron microscopy and Raman spectroscopy, respectively. After laser irradiation, disordered sputtered surface with intense melting and cracking is obtained at the central ablated areas, which are augmented with increasing laser fluence due to enhanced thermal effects. At the peripheral ablated areas, where local fluence is approximately in the range of 1.4–4 mJ cm^{-2}, very well-defined laser-induced periodic surface structures (LIPSS) with periodicity ranging from 270 to 370 nm along with dot-like structures are formed. As far as the pulse duration is concerned, a significant effect on the surface modification of Cr has been revealed. In the central ablated areas, for the shortest pulse duration (25 fs), only melting has been observed. However, LIPSS with dot-like structures and droplets have been grown for longer pulse durations. The periodicity of LIPSS increases and density of dot-like structures decreases with increasing pulse duration. The chemical and structural modifications of irradiated Cr have been revealed by Raman spectroscopy. It confirms the formation of new bands of chromium oxides and enol complexes or Cr-carbonyl compounds. The peak intensities of identified bands are dependent upon laser fluence and pulse duration.

Keywords: chromium; femtosecond laser; pulse duration; fluence; nanostructures; laser-induced period surface structures; SEM; Raman spectroscopy

1. Introduction

During the past 15 years, ultrashort (femtosecond (fs)) lasers have been demonstrated as a high precision and powerful micro/nanostructuring tool for materials processing (*1–5*). These lasers form a relatively small heat-affected zone and less mechanical and thermal damages. In contrast to material processing using nanosecond or longer laser pulses where standard modes of

*Corresponding author. Email: shaziabashir@gcu.edu.pk

thermal processes dominate, fs laser pulses can induce nonthermal structural changes, driven by electronic excitation, plasma formation and associated nonlinear processes. Predicting the topography on metallic surfaces generated by fs laser pulses is a challenging task since there are several physical mechanisms which are responsible for the energy deposition process (*5–7*).

The self-organized nano as well as micro-periodic structures, known as ripples, have been observed on laser-irradiated surfaces even from the beginning times of laser processing of materials (*8*). The origin of the laser-induced periodic surface structures (LIPSS) is still debatable and has been discussed in the literature extensively (*4,8–11*). A lot of experimental parameters has been revealed to have influence upon the periodicity of the laser-induced surface structures, such as material refractive index as well as threshold, laser fluence, number of laser pulses, pulse duration, laser wavelength, radiation polarization and incidence angle. Taking into account their typical dimensions, two main types of ripples are distinguished in the literature. The first type is called low spatial frequency LIPSS (LSFL) with spatial periods close to or slightly lower than the laser wavelength. To explain the formation of ripple periods near the laser wavelength, a theoretical description on the basis of the excitation of an electromagnetic surface wave interfering with the light field was given by Sipe and co-workers (*9*). Huang et al. (*12*) have studied several different materials including silicon and used the surface plasmon polariton (SPP) concept along with numerical simulation to explain their experimental finding of the pulse number dependence of the LIPSS periods upon irradiation by fs-laser pulses (1280 nm wavelength, 125 fs).

Nanostructures grown by fs laser irradiation on metallic surfaces have novel technological applications in optoelectronics, biology and medicine. These structures are ideal model systems that merge the concepts known from photonic crystals (*13*) with the exceptional material properties of metals to form ‘plasmonic crystals’. Surface plasmons are used to enhance Raman scattering, molecular fluorescence, field-enhanced electron generation, the output efficiency of solid-state light emitters and Terahertz lasers (*14*). This opens the door for various new applications in nanoimaging and spectroscopy. A specific example is the imaging of nanometresized domains in polymers (*15*) or magnetic materials.

The formation of micro/nano structures (ripples, columns and cones) on bulk as well as on thin films by multiple pulse laser irradiations has been reported by several research groups (*4,8–11,16*). The growth of these structures in the presence of liquids is significantly important for technical and medical applications, *e.g.* laser shock processing, nanoparticle formation, microstructure fabrication and dental tissue ablation. The laser matter interactions in liquids involve complex processes such as laser-induced cavitations bubble, explosive boiling, the confinement effect, cooling due to heat conduction, an enhanced nucleation and chemical reactivity. These processes play a significant role in liquid-assisted ablation (*17–19*).

From the basic evolution processes of the laser-induced plasma in a confining liquid, two condensations of the plasma plume in the liquid can find their applications in materials synthesis, one for the nanocrystal fabrications and the other for the surface coating preparation (*20*). Nano structures of metals and their alloys, oxides, nitrides and carbides can be prepared by laser ablation of solids in liquids (*21*). Additionally, laser ablation of solids in liquids is a technique developed for ‘steam laser cleaning’ to remove micrometer and submicrometer particles from the surface of metals and semiconductors, which shows high potential in microelectronics (*22–24*). The previous work reported by our group (*16*) deals with the irradiation of stainless steel at various fluences by multiple fs laser pulses (25 fs pulse duration, 800 nm central wavelength, 1 kHz pulse repetition frequency) in air and liquids (water and ethanol).

The motivation behind the current research work is to explore the optimum and favorable conditions for the growth of micro- and nanostructures on the surface of Cr after fs laser irradiation. Parametric studies are carried out to reveal various ablation phenomena in Cr by varying the laser fluence and pulse durations with emphasis on melting and formation of nanoscale LIPSS in central as well as peripheral ablated areas. Experiments are conducted for ablation of Cr in

ethanol environment at an near infrared wavelength using a Ti:Sapphire fs laser. The innovative aspect of the present work is that according to our best knowledge no work is reported in which effect of varying fluence as well as pulse duration of fs laser on the growth of LPSS of bulk Cr after ablation in ethanol has been investigated by both scanning electron microscope (SEM) as well as Raman spectroscopy analyses. The parametric dependency of LIPSS and its correlation with structural modification of ethanol-assisted ablated bulk Cr have not been established. Laser parameters employed in the present study such as fluence corresponding to peak laser fluence ranging from 4.7 to 11.8 and local fluences ranging from 1.4 to 4 mJ cm^{-2} as well as and pulse duration ranging from 25 to 100 fs have not been explored The previously reported work by Albu et al. (*25*) deals with growth of LIPSS on the metallic films with thickness of about 200–230 nm at constant pulse duration of 200 fs and with fluence variation from 0.06 to 0.18 J cm^{-2}.

2. Experimental details

Mechanically polished and ultrasonically cleaned chromium (Cr) samples of dimension $15 \times 15 \times 3\ mm^3$ were used as target. The schematic of experimental set-up is shown in Figure 1. The samples were mounted on the motorized xyz manipulator to position the targets precisely for each exposure. The irradiation was performed by using Chirp Pulse Amplification Ti:Sapphire laser system. The system was operated at a repetition rate of 1 kHz with a central wavelength of 800 nm. A lens with a focal length of 17 mm was used to focus the laser beam onto the target surface. The exposures were performed in an ethanol environment by placing the targets 5 mm after the focus position where the spot size was measured to be 36 µm. This arrangement is used to enhance the chemical and structural modifications of irradiated Cr in ethanol environment which is revealed by Raman spectroscopy. The breakdown in ethanol generates high temperature and pressure. If the temperature of liquid approaches its critical temperature, the initiation of phase explosion develops and the superheated liquid region (metastable) is formed. This region is initiated by homogenous multiple-bubble formation accompanied by shockwave generation. Therefore, this process validates the expectation of explosive liquid vaporization. The confinement of plasma expansion in the liquid layer intensified acoustic pressure and increased shockwave duration, owing to the additional photomechanical effects consequently promoting material removal efficiency (*26*).

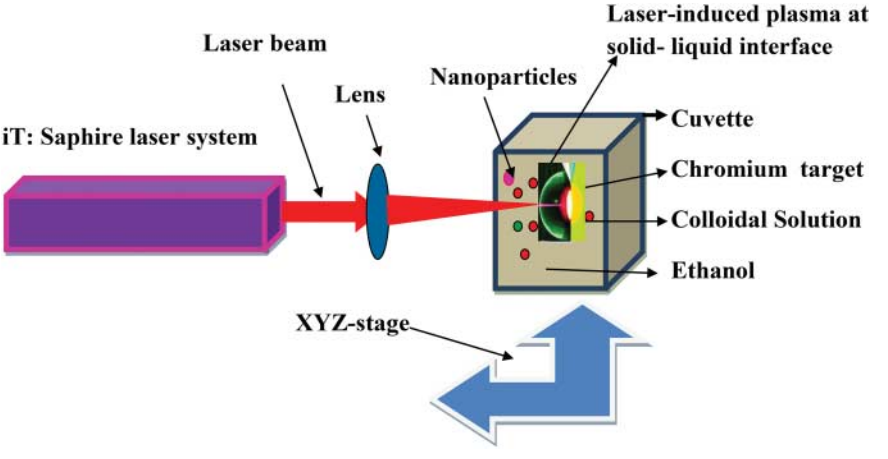

Figure 1. The schematic of the experimental set-up for exposure of Cr by fs laser pulses in an ethanol environment.

The first part of the experiment was performed by exposing the Cr targets in the ethanol environment to four different pulse energies of 200, 300, 400 and 500 µJ, while keeping the pulse duration constant at 25 fs. These energies were measured by the power/energy meter before the cuvette. The measured values of laser pulse energies after passing through the cuvette filled with ethanol turned out to be 186, 279, 372 and 460 µJ. The average pulse energies hitting the Cr target turned out to be 193, 290, 386 and 480 µJ. The peak fluence values corresponding to average pulse energies with focal spot size of 36 µm are 4.7, 7.1, 9.4 and 11.8 J cm^{-2}. The local fluences at the peripheries at a distance of 100 µm from center, where growth of LIPSS is observed, have been evaluated by using the following relation (*27*):

$$\phi_{\min} \approx \phi_o \exp\left[-\frac{1}{2}\left(\frac{D_{\mathrm{LIPSS}o}}{\omega_0}\right)^2\right], \tag{1}$$

where $\phi_{\min}$ is the local fluence, ϕ_o is the peak fluence, $D_{\mathrm{LIPSS}o}$ is the diameter of peripheral region (200 µm for presnt case), where LIPSS are observed and ω_0 is the beam waist. The evaluated values of local fluences are 1.4, 2.4, 3.1 and 4 mJ.cm^{-2}. These values are illustrated in the table.

In the second part of the experiment, the targets were exposed in the ethanol environment to three pulse durations of 25, 50 and 100 fs keeping the fluence constant at 600 µJ. The variation in pulse duration was achieved by using the Acousto-Optic Dazzler system (Electro Optics France). It is an Acousto-Optic Programmable Dispersive Filter composed of an acousto-optic crystal and radio frequency generator which is designed to filter ultrafast laser pulses. It performs convolution between amplitude of the input signal and the programmable acoustical signal.

The pulse duration after Group Delay Dispersion (GDD) is

$$\tau = \tau_0 \sqrt{1 + \left(4\ln 2 \frac{\mathrm{GDD}}{\tau_0^2}\right)^2}, \tag{2}$$

where τ_0 is the minimum pulse duration and τ is the pulse duration after GDD.

The pulse duration of the laser beam was measured by a dispersion-minimized auto correlator (Femtometer, Femtolasers Produktions, Vienna, Austria).

When beam focus passes through ethanol, various nonlinear effects (*28*) as well as filamentation and self-phase modulation occur. Of course all these phenomena are responsible for broadening of the spectrum inside the liquid. During experimentation the only possibility is to measure the pulse duration of the beam before passing through the liquid. The measurement of pulse duration exactly at the sample's surface when it was dipped into the liquid and is inside the cuvette is not possible. Therefore, various phenomena such as nonlinear effects, filamentation and self-phase modulation causing pulse stretching inside the liquids can be considered additional effects induced by liquid during ablation of Cr.

The targets were exposed to1000 succeeding pulses for both sets of the experiment. The separation between each spot is 2 mm. This distance is sufficient to avoid overlapping.

The surface morphology of the irradiated was analyzed by using an SEM (FEI-QUANTA 200F, the Netherlands). SEM analysis was performed for both central and peripheral ablated areas of Cr. To explore the structural characteristics of ablated targets, micro Raman spectroscopy was performed using a Raman spectrometer Lab Ram HR-800 (Horiba Jobin-Yvon) with a spectral resolution of 3 cm^{-1}. An He–Ne laser operated at 632.8 nm with 8 mW was used as an excitation source. Raman spectroscopy was performed in backscattering geometry. The spectral data were accumulated at a fixed grating position for one minute and were collected using an air-cooled charged coupled device camera.

3. Results and discussion

3.1. *SEM analysis*

SEM image of Figure 2(a) shows the overall ablation spot on the Cr surface after ablation at the lowest fluence. Its relevant zoomed sections for central as well as peripheral ablated areas are also labeled and are illustrated in Figure 2(b) and 2(c).

3.1.1. *Effect of laser fluence on the surface of ethanol-assisted fs laser-ablated Cr*

SEM images in Figure 3 display the surface morphology of central ablated areas of Cr at various fluences of (a) 4.7, (b) 7.1, (c) 9.4 and (d) 11.8 J cm^{-2} The disordered sputtering, melting and cracking are observed for all pulse energies. However, the efficacy toward melting as well as cracking increases with increasing energy due to enhanced thermal effects. At the lowest fluence of 4.7 J cm^{-2} (Figure 3a) there seems to be less sputtering with large number of small-sized droplets. When the fluence increases to 7.1 J cm^{-2} both the sputtering and cracking increase (Figure 3(b)), but the density of droplets decreases significantly. For the fluence of 9.4 and 11.8 J cm^{-2}, it is seen in Figure 3(c) and 3(d) that both cracking and melting become dominant due to enhanced thermal ablation mechanisms (*29*) and phase explosion (*30*).

As the material undergoes multiple laser pulse irradiation in the ethanol environment, there is a possibility for the generation of thermal stresses (*31*). These stresses are accumulated on

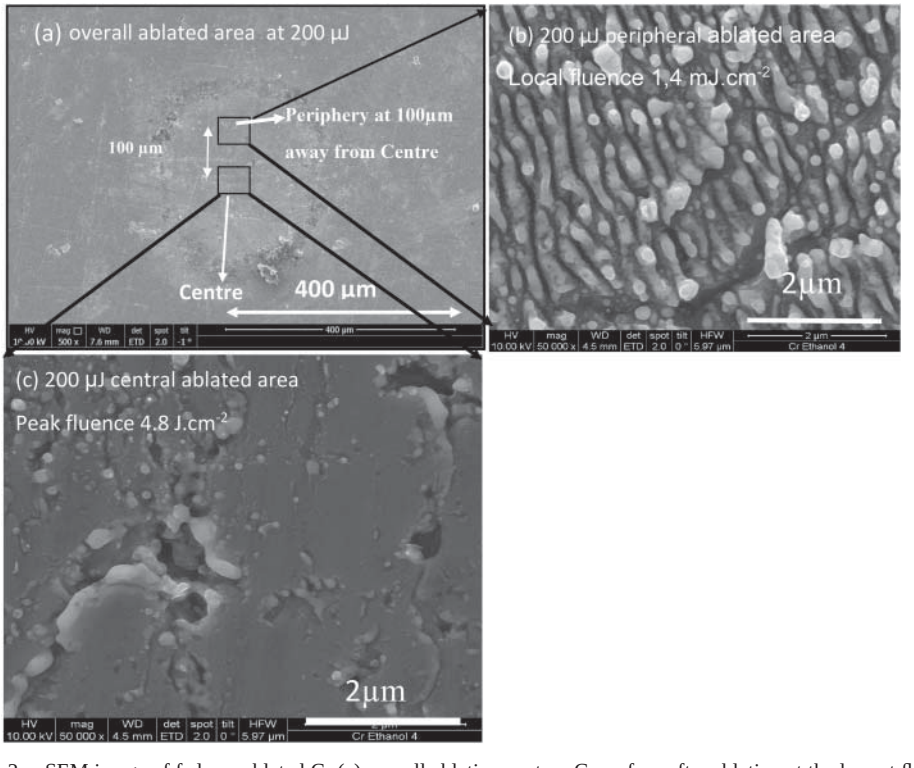

Figure 2. SEM image of fs laser-ablated Cr (a) overall ablation spot on Cr surface after ablation at the lowest fluence of 4.7 J cm^{-2}. Relevant marked zoomed sections (b) central ablated area and (c) peripheral ablated areas.

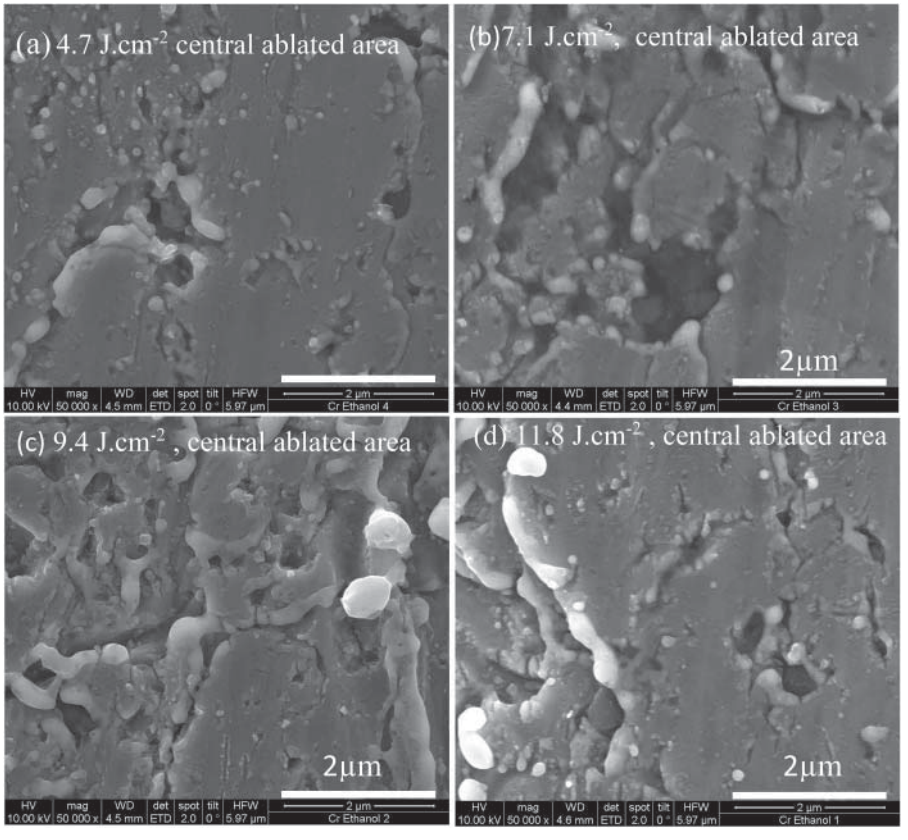

Figure 3. SEM images revealing the cracking and melting with nonuniform surface structures at the central ablated areas after exposure of Cr to 1000 fs laser pulses at pulse duration of 25 fs for various fluences of (a) 4.7, (b) 7.1, (c) 9.4 and (d) 11.8 J cm^{-2}.

the irradiated sites resulting in material fracture and crack formation as shown in Figure 3(a)–(d) (*10*).

SEM images of Figure 4 illustrate the surface morphology of peripheral ablated areas of Cr at various local fluences of (a) 1.4, (b) 2.4, (c) 3.1 and (d) 4 mJ cm^{-2}. Very well-defined and organized LIPSS are grown for all fluences at the boundaries. The average periodicity of LIPSS varies from 270 to 370 nm for various lacl fluences.

The periodicity of LIPSS increases from 350 to 370 nm with increasing fluence from 1.4 to 3.1 mJ cm^{-2} and then decreases to 270 nm at a maximum fluence value of 4 mJ cm^{-2}. It is also found that the appearance of LIPSS becomes more organized and distinct with increasing laser fluence. Table 1 illustrates the values of pulse energies and corresponding values of peak fluences as well as local fluences at a distance of 100 µm from the center, where LIPSS are observed which is considered as the peripheral ablated area. The dot-like structures with an average diameter of 200 nm have also been observed lying at the top of the LIPSS.

The growth of LIPSS is thought to be the result of the interaction of surface plasmons or surface waves with the incoming electromagnetic radiation (*5*,*32*–*34*). Several authors have proposed the excitation of SPPs as the possible mechanism responsible for the surface wave generation in metals, semiconductors and dielectrics.

Once a high free electron density is produced by multiphoton ionization, the material has the properties of plasma and will absorb the laser energy via one-photon absorption mechanism of

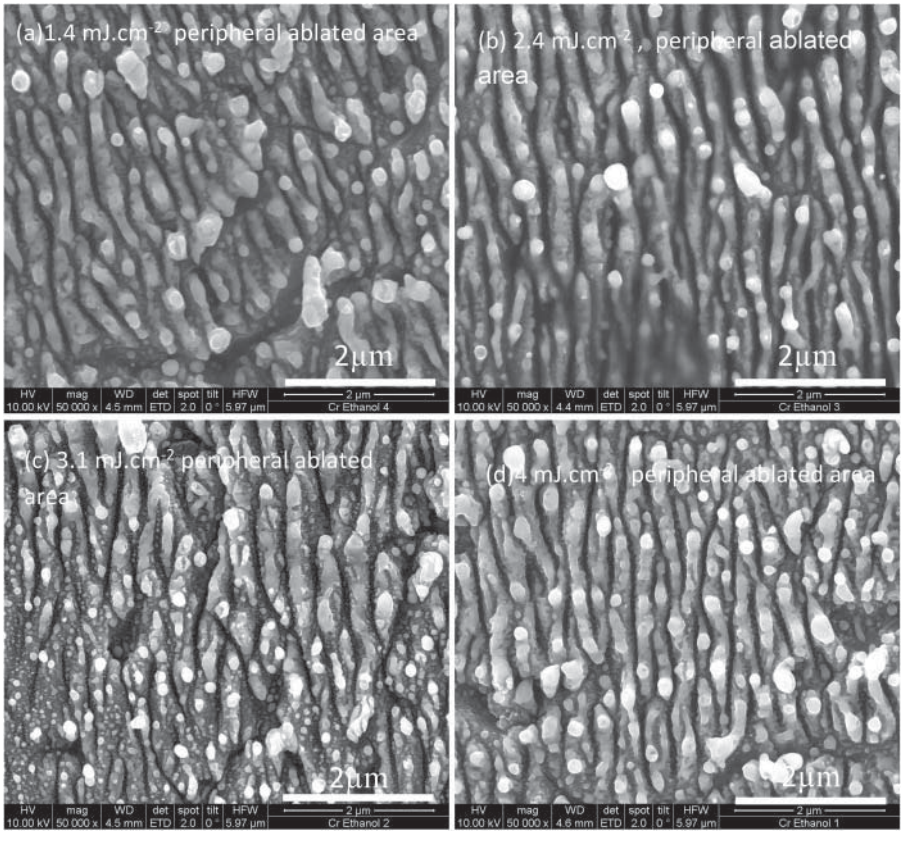

Figure 4. SEM images revealing the formation of laser-induced periodic surface structures at the peripheral ablated areas after exposure of Cr to 1000 fs laser pulses at pulse duration of 25 fs, at various local fluences of (a) 1.4 , (b) 2.4, (c) 3.1 and (d) 4 mJ cm^{-2} in an ethanol environment.

inverse bremsstrahlung (joule) heating. The light absorption in the electron plasma will excite bulk electron plasma density waves. These are longitudinal waves with the electric field component parallel to the laser polarization. In the present study, LIPSS are observed on the Cr surface after ablation in ethanol with a periodicity ranging from 270 to 370 and their orientation is perpendicular to the laser polarization (*35*). The SPP mechanism explains why the orientation of the periodic structures is perpendicular to the laser polarization direction of propagation. Such an electron plasma wave could couple with the incident light wave only if it propagates in the plane of light polarization. Initial coupling is produced by inhomogeneities induced by electrons moving in the plane of light polarization (*10*).

SPPs result from the coherent interaction of the incident laser field with free electrons created in the material (*36*). The formation of laser-induced nanogratings is not determined by the physical properties of materials at normal state but the high excited state induced by ultrafast laser irradiation with the fluence near the ablation threshold. With this irradiation condition, in an ultrashort timescale, abundant electrons are excited and high-density plasmas are produced, which will change the surface physical properties of the material significantly (*37*). The spatial frequencies of the plasmons which directly determine the ripple periods are a function of the fluence-dependent density of free carriers (*38*).

As a general tendency the periodicity of ripples increases with increasing laser energy (*10*). When the material is irradiated by a focused fs laser beam, multiphoton absorption and

Table 1. The periodicity of LIPSS grown at peripheral ablated areas at different pulse laser energies and fluences for chromium irradiated with 1000 fs laser pulses at wavelength of 800 nm and pulse duration of 25 fs in an ethanol environment.

Laser pulse before cuvette (μJ) A1	Laser pulse energy after passing through a cuvette filled with ethanol (μJ) A2	Average laser pulse energy (μJ) hitting the Cr surface (average of A1 and A2)	Peak laser fluence (ϕ_o) (J cm^{-2})	Local fluence (J cm^{-2}) $\phi_{\min} \approx \phi_o \exp\left[--\frac{1}{2}\left(\frac{D_{\mathrm{LIPSSo}}}{\omega_0}\right)^2\right]$ (27)	Experimental periodicity of LIPSS (nm)
200	186	193	4.7	1.4	350
300	279	290	7.1	2.4	360
400	372	386	9.4	3.1	370
500	460	480	11.8	4	270

Table 2. The comparison between experimental periodicity of LIPSS and calculated periodicity from different predictions such as interference theory as well as surface plasmon's theory chromium sample for laser wavelength of (λ) 800 nm.

Environment	Refractive index n_{env}	Experimental periodicity of LIPSS by 800 nm $\approx \Lambda$ (nm) (in the present study)	Experimental periodicity of LIPSS $\approx \Lambda$ (nm) reported by Albu et al. by 775 nm	Periodicity of LIPSS by interference theory: The thresholds of surface nano-/micro-morphology modifications with fs laser pulse irradiations, $\Lambda = \frac{\lambda}{n_{\mathrm{env}}}$ (nm)	Periodicity of LIPSS by surface plasmon's theory: $\Lambda_{\mathrm{SP}} = \lambda \mathrm{Re}[((\varepsilon_{\mathrm{d}} + \varepsilon_{\mathrm{m}})/(\varepsilon_{\mathrm{d}}\varepsilon_{\mathrm{m}}))^{1/2}]$, where λ is laser wavelength, ϵ_{d} refers to the permittivity of the dielectric medium and $\epsilon_{\mathrm{m}} = \epsilon_{\mathrm{r}} + i\epsilon_{\mathrm{i}}$ is the complex dielectric constant of the metal (nm)
Air	1	Not measured	460–550	800	578 (25)
Ethanol	1.36	270–370	120–180	588	216 (25)

photoionizations occur. Thus, the electron plasma is created in the material, characterized by the electron plasma temperature (T_e) and the plasma density (N_e). An analytical expression for the periodicity (Λ) of LIPSS versus electron temperature (T_e) and density (N_e) proposed by Shimotsuma et al. (*10*) is as follows:

$$\Lambda = \frac{2\pi}{\sqrt{1/T_e((m_e\omega^2/3k_B) - (e^2N_e/3\omega k_B)) - k_{pp}^2}}, \tag{3}$$

where m_e is an electron mass, k_B the Boltzmann constant and ω the angular frequency. This dependence shows that the grating period increases with the increase of electron concentration and electron temperature. But it could be extracted from the above expression that plasma parameters have a nonlinear effect on ripples grating. Therefore, when the laser energy initially increases, the photoelectrons created by multiphoton photoionization process are more energetic and the electron plasma temperature increases. Following the dependence of the ripples' periodicity on the electron plasma temperature from relation (1), the periodicity of ripples increases as has been observed.

Characteristics of the laser-produced plasma strongly depend on the laser irradiance levels (*39*). It is reported in the literature (*40*,*41*) that up to a certain value of laser irradiance both the plasma parameters, *i.e.* electron temperature and number density, increase with increasing laser irradiance due to enhanced energy deposition. With further increase in irradiance a shielding occurs and can be explained only on the prominent absorption mechanisms via inverse bremsstrahlung and photoinization as well as self-absorption of plasma (*41*). The expansion of the plasma causes its cooling due to condensation, recombination and diffusion within the plasma volume. This causes reduction in the plasma temperature and density.

With increasing laser fluence, it can be assumed that a large amount of the absorbed laser energy is mainly converted to heat, leading to some well-known phenomena such as melting. In this case, the surface temperature may also be modulated by the deposited (inhomogeneous) energy formed by interference (incident-scattered). When the temperature is increased, the gradient of the surface tension results in a shear force, which causes the movement of hot liquid toward cold regions to minimize its energy and the surface deformation. Therefore, the consequence of these effects can be considered one reason for the change of the periodicity of LIPSS.

The irradiation at the ethanol–Cr interface increases the temperature high enough (due to confinement) that it induces a phase change of Cr. Thus, bubble formation/collapse in the ethanol layer impinges upon the Cr and creates LIPSS or ripples on the surface (*31*,*42*). In addition to that, this bubble expansion/collapse precipitates the convective flow of the Cr molten layer due to variations in surface tension (thermocapillary effect) of the material (*31*,*42*). These variations are responsible for inducing increased hydrodynamic instabilities called Kelvin–Helmholtz and pressures at the liquid–solid interface (*43*).

In a multi-shot regime, the fluence threshold evolves differently depending on the number of laser shots and the material characteristics. The process of LIPSS formation can be described by interference of the incident laser beam with some form of a surface-scattered electromagnetic wave (*44*). Sipe's theory provides a mathematical expression for the inhomogeneous absorption of the radiation energy in the laser-irradiated material. Based on this theory, Bonse and Kruger (*27*) gave detailed analysis of the pulse number dependence of the distribution of the spatial frequencies and the corresponding spatial periods, revealing that the total number of laser pulses are crucial and can be used for controlling the periodicity of LIPSS. Namely, the interference of the electric field of the SPP with the incident laser beam leads to a spatially modulated energy deposition in the material and finally generates the LSFL via inhomogeneous ablation. According to Huang et al. (*12*) the decrease in the LSFL period for an increasing number of laser pulses occurs via a grating-assisted surface plasmon–laser coupling. As the grating-like LSFL surface relief

formed during firstfew laser pulses deepens, the resonant wavelength of the SPP will undergo a red shift. This leads to a decrease in the LFSL periods during the multipulse feedback phase.

In a previous study, Huynh and Semmar (*35*) determined the incubation coefficient for Cu and found that the ablation threshold decreases with respect to the number of coincident laser shots. With multi-shot laser irradiation of the same surface spot, the incubation effect can change the absorption of the material by evaporation of the top layer of the surface (*i.e.* every new pulse irradiates a modified surface profile, causing further mass removal) (*35*). This reduction is due to the accumulation effect induced by thermal stress–strain energy storage (*45*).

The dot-like structures or droplets are formed due to colloidal formation or nucleation process under extreme conditions of high-temperature–high-pressure plasma at the liquid–solid interface (*20*). The Cr clusters are formed in the cavitation bubbles that are generated during the laser breakdown. The adiabatic expansion as well as cooling of Cr plasma plume react with ethanol and enhance its chemical reactivity. The size variation is dependent upon the energy deposition by the laser and structural (chemical) modifications (various oxides or enol complexes) (*20*).

The comparison between experimental periodicity of LIPSS and calculated periodicity from different predictions such as interference theory as well as surface plasmon's theory for chromium sample is illustrated in Table 2. The table also provides the comparison with previously reported work on Cr by Albu et al. (*25*).

The work reported by Albu et al. (*25*) was related to growth of LIPSS on the metallic films with thickness of about 200–230 nm. The laser wavelength of 775 nm was used. The periodicity of LIPSS determined from 2D-FT measurements is 120–180 nm in case of ethanol. Metallic surfaces were processed by scanning at a scan speed of 1 mms^{-1} with corresponding overlap (OL) between subsequent laser pulses in the range of 93% and 96%. The laser fluence was varied between 0.06 and 0.18 J cm^{-2}. However, the present work deals with growth of LIPSS on bulk Cr with laser wavelength of 800 nm. All exposures were performed in an ethanol environment by placing the targets 5 mm after the focus position with 1000 number of laser pulses at local fluence ranging from 1.4 to 4 mJ cm^{-2}. The LIPSS period varies from 270 to 370 nm. The higher values of observed periodicity values of LIPSS for present case are attributable to difference in number of overlapping laser pulses (1000 in our case), position of the target from the focus position (5 mm away), slightly higher value of wavelength (800 nm), shorter pulse duration (25 fs) and nature of material (bulk).

The formation mechanism and the LIPSS period could be explained within the surface plasmon theory (*12*). The interference between the incident laser light and the excited surface plasmons wave created at the dielectric–material interface will cause a periodic intensity variation on the surface, and a periodical thermal gradient is created. Due to the thermocapillary forces induced by the thermal gradient, the melted material moves from the hot region to the colder region (Marangoni effect); then periodical structures are formed by a self-organized process.

According to the two-temperature model, diffusion of hot electrons results in faster equilibration times between hot electrons and the lattice. Therefore, the lattice temperature exceeds the melting temperature faster in thick photoexcited samples than in thin films, and so the solid-to-liquid transition should occur more quickly in thicker samples (*46*).

3.1.2. *Effect of pulse duration on the surface of ethanol-assisted fs laser-ablated Cr*

A significant effect of pulse duration on the surface modification of Cr has been observed in SEM images of Figure 5(a)–(f). Micrographs of Figure 5(a), 5(c) and 5(e) correspond to modified surface of Cr at central ablated areas at a fluence of 11.8 J cm^{-2}, whereas micrographs in Figure 5(b), 5(d) and 5(e) denote peripheral ablated areas at a fluence of 4 mJ cm^{-2}. In the central ablated areas, only melting and cracking have been observed for the shortest pulse duration

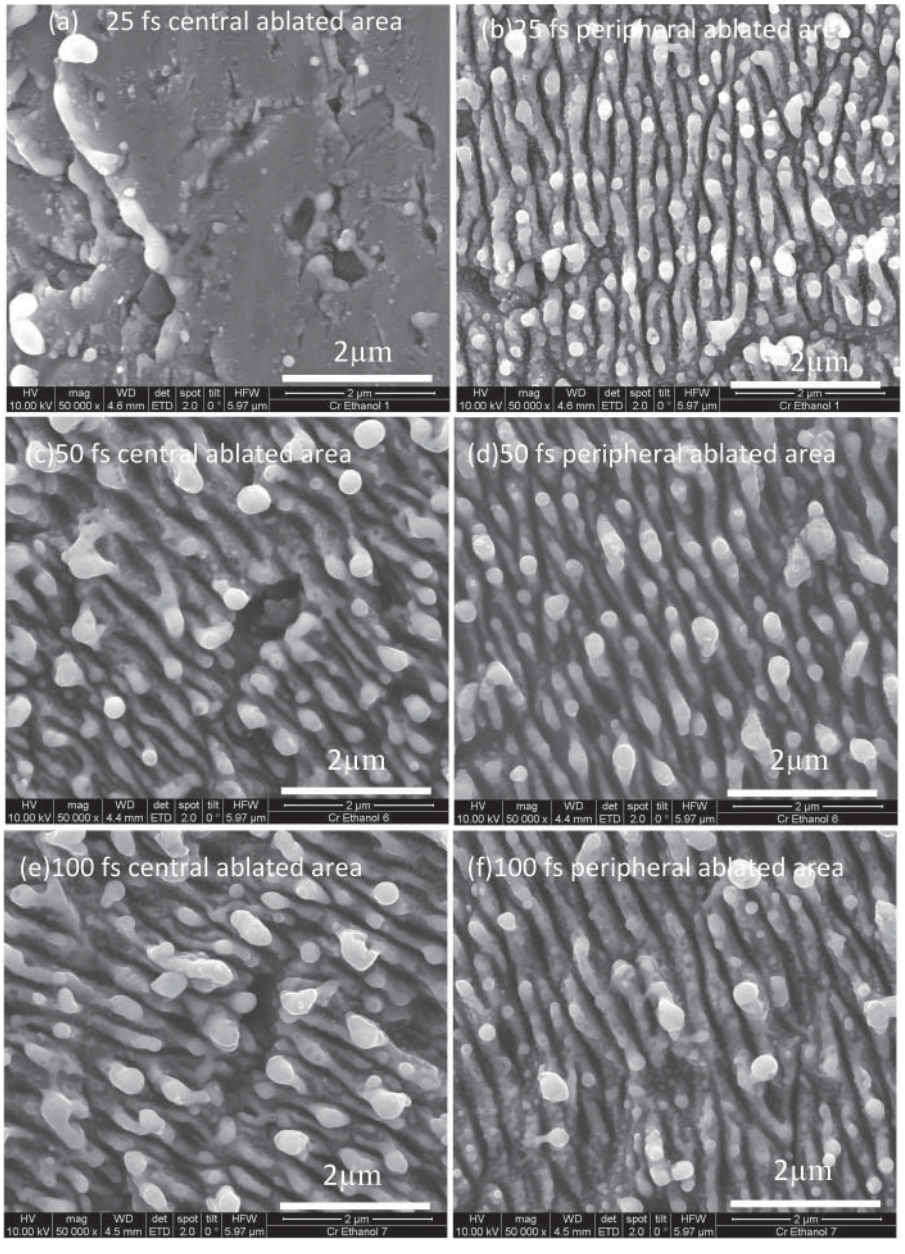

Figure 5. SEM images revealing the central as well as peripheral ablated areas resulting from the exposure of Cr to 1000 fs laser pulses at a fluence of 11.8 J cm^{-2}, for various pulse durations of (a) 25 fs, center, (b) 25 fs, periphery, (c) 50 fs, center (d) 50 fs, periphery (e) 100 fs, center and (f) 100 fs, periphery, in an ethanol environment. In the central ablated area, only melting and cracking have been observed for the shortest pulse duration of 25 fs. For the pulse durations of 50 fs as well as of 100 fs, well-defined LIPSS with dot-like structures and droplets have been grown.

of 25 fs (Figure 5(a)). For the pulse durations of 50 fs (Figure 5(c)) and 100 fs (Figure 5(e)), a significant difference in the surface morphology is revealed. Instead of melting and cracking, well-defined LIPSS with dot-like structures and droplets have been grown. The appearance of LIPSS is more distinct and organized. The size of dot-like structures increases with increasing pulse duration. Phase ejection, fragmentation, homogeneous nucleation, agglomeration and

Table 3. The periodicity of LIPSS grown at peripheral ablated areas at different pulse duration energies for chromium irradiated with 1000 fs laser pulses at a wavelength of 800 nm and at a local laser fluence of 4 mJ cm^{-2}.

Laser pulse duration (fs)	Experimental periodicity of LIPSS (nm)
25	270
50	290
100	330

spinodal decomposition (*47*) are the main causes for the growth of dot-like structures. During ultrashort laser pulse irradiation, the energy is delivered to matter in such short a timescale that absorption occurs at nearly solid-state density (nearly isochoric heating). The laser energy is first deposited in the electronic subsystem within a superficial layer with a thickness of tens of nm. Then, the energy is rapidly transferred from the electrons to the lattice, and the heated region can reach high temperatures which are accompanied by a build-up of strong pressures within the material (*47*). The process of energy deposition by thermal conduction becomes dominant for comparatively longer pulses (50 and 100 fs) as compared to shorter pulses (25 fs) for our case. Therefore, the size of dot-like structures increases with increasing pulse duration.

For peripheral ablated areas LIPSS with dot-like structures are formed for all pulse durations ranging from 25 to 100 fs (Figure 5(b), 5(d) and 5(f)). The periodicity of LIPSS and size distribution of dot-like structures increase and the density of dot-like structures decreases with increasing pulse duration.

It is observed that for the shortest pulse duration of 25 fs, LIPSS have been developed only at the peripheries where energy deposition is smaller. In the central ablated areas only cracking and melting occurs which is due to more energy deposition. For pulse duration of 25 fs, the intensity of the laser beam is higher as compared to that of longer pulses of 50 and 100 fs. Therefore, high temperatures are accompanied by a build-up of strong pressures within the material. These extreme pressures and temperatures are responsible for nonuniform ablation. When pulse duration increases, laser intensity decreases and nearly adiabatic vacuum expansion of the heated material occurs with a consequent decrease of density and temperature. At this stage, the evolution of the system during this relaxation from the extremely excited state mainly depends on the level of laser irradiation intensity and causes LIPSS formation (*47*). In case of longer pulse durations of 50 and 100 fs, the growth of LIPSS is observed for both central as well as peripheral ablated areas and it confirms the less energy deposition due to smaller intensities at centers for longer pulses as compared to shorter pulses. Table 3 illustrates the values of periodicity of LIPSS for various pulse durations at a fluence of 4 mJ cm^{-2}.

Femtosecond-pulsed laser interaction triggers a variety of timescale processes influenced by the fluence and pulse duration (*48–50*). For very short laser pulses (fs), energy absorbed by the electrons is much faster than it is transferred to the lattice (*51*). Since the lattice does not heat appreciably during the pulse, there is no modification of electron-lattice scattering rates. Therefore, with pulses of duration less than 50 fs nonthermal phenomena are dominant over thermal processes (*52*).

3.2. *Raman spectroscopy analysis*

Raman spectroscopy is widely used for the analysis of structural and phase disorder information related to metallic oxides and metallic carbonyl compounds. In the presence of liquids, the chemical reactivity of the target with liquid is significantly enhanced which is responsible for the growth of new phases and modification in the chemical composition of the irradiated target.

3.2.1. *Effect of fluence on ethanol-assisted fs laser-ablated Cr*

Raman spectrographs in Figure 6 show the structural modifications in the Cr after its exposure to 1000 laser pulses for various fluences ranging from 4.7 to 11.8 J cm^{-2} for a pulse duration of 25 fs in ethanol. Figure 6 also clearly indicates that the increase in surface roughness is responsible for enhanced intensity of Raman signal. Two strong peaks are identified at wavenumbers of 1274 and 1534 cm^{-1} for the exposures for all pulse energies. These bands correspond to C–C stretching vibration or enol complexes (*53*). As the material undergoes multiple laser pulses, in an ethanol-confined environment, there is a possibility of oxide formation. These oxides are identified on the irradiated surface of Cr in the form of tiny Raman peaks Cr_8O_{21} (246 cm^{-1}), Cr_2O_5 (253 cm^{-1}), Cr_8O_{21} (487 cm^{-1}), Cr_2O_7 (515 cm^{-1}) and Cr_2O_3 (550 and 610 cm^{-1}) (*43*), resulting in material modification.

With increasing fluence, initially the peak intensities of corresponding bands of Cr oxides and Cr enol complexes increase up till 9.4 J cm^{-2}. It indicates that these bands become strong with increasing pulse energies. However, for the maximum fluence of 11.8 J cm^{-2}, the bond dissociation takes places due to an enhanced thermal effect which is responsible for degradation of peak intensities of these bands. For a fluence of 9.4 J cm^{-2}, the density distribution of droplets or dot-like structures is maximum and afterwards it decreases again for the maximum fluence of 11.8 J cm^{-2}. It shows that Raman results are compatible with SEM analysis.

The extreme pressure and temperature conditions in the focal volume during laser ablation enhance the chemical reactivity of Cr with dissolved oxygen in ethanol and support the formation of various kinds of oxides (*20*). The shockwave that results from the laser breakdown generates high pressure–high temperature conditions at the liquid–plasma interface, which becomes an active chemical reaction zone that enhances the bonding of Cr species with ionized ethanol molecules to form Cr oxide nanostructures.

3.2.2. *Effect of pulse duration on ethanol-assisted fs laser-ablated Cr*

Raman spectrographs in Figure 7 show the structural modifications in the Cr after its exposure to1000 laser pulses at various pulse durations ranging from 25 to 100 fs in ethanol at a fluence of 11.8 J cm^{-2}.

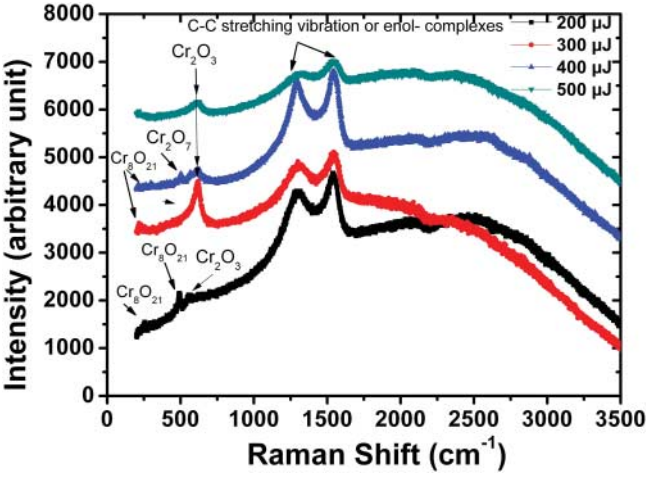

Figure 6. Raman spectra for fs laser-irradiated Cr exposed to 1000 succeeding pulses of various fluences ranging from 4.7 to 11.8 J cm^{-2} for pulse duration 25 fs, in an ethanol environment. Cr enol complexes as well as various kinds of chromium oxides are formed.

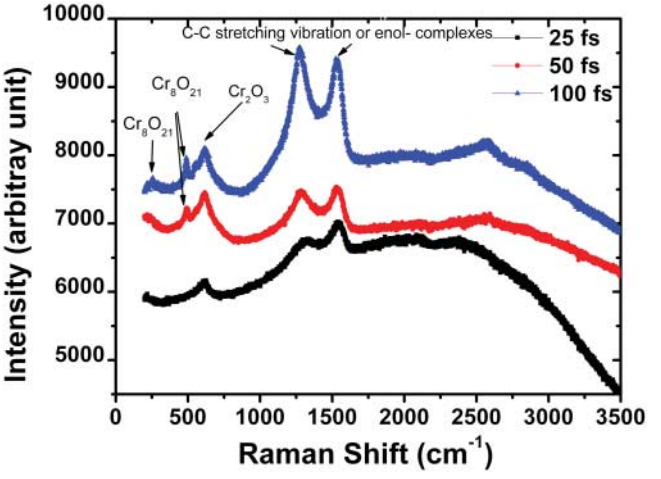

Figure 7. Raman spectra for fs laser-irradiated Cr exposed to 1000 succeeding pulses at a fluence of 11.8 J cm^{-2}, in an ethanol environment for various pulse durations ranging from 25 to 100 fs. Cr enol complexes as well as various kinds of chromium oxides are formed.

Two strong peaks are identified at wavenumbers of 1274 and 1534 cm^{-1} for the exposures for all pulse durations. These bands correspond to C–C stretching vibration or ethanol complexes (*53*).

For all pulse durations ranging from 25 to 100 fs two peaks are identified at wavenumbers 246 and 610 cm^{-1}. These peaks represent oxides formation of Cr, *i.e.* Cr_8O_{21} and Cr_2O_3 (*53*), respectively. With increasing pulse duration to 50 and 100 fs a Raman peak corresponding to wavenumber 487 cm^{-1} is also observed. This peak corresponds to Cr_8O_{21}.

As far as the pulse duration is concerned, a significant increase in the peak intensities of identified bands is observed with increasing pulse duration which is also attributable to enhanced chemical reactivity Cr with ethanol and oxygen for longer pulses.

4. Conclusions

The surface and structural modification in Cr by fs laser irradiation in an ethanol environment is dependent on pulse energies and pulse durations. The central ablated areas exhibit cracking and melting because of thermal effects whereas at the peripheries LIPSS are the dominant features. LIPSS turn out to be more organized and distinct with the increase in the pulse energies. As far as the effect of pulse duration is concerned, LIPSS with dot-like structures and droplets have been grown for 50 and 100 fs durations except 25 fs where there is a nonuniform ablation. However, LIPSS are grown in peripheral ablated areas for all pulse durations. Raman spectroscopy reveals that the ethanol environment forms the enol complexes of Cr or C–C stretching as well as oxide formation of Cr.

Disclosure statement

No potential conflict of interest was reported by the authors.

References

(1) Bashir, S.; Rafique, M.S.; Husinsky, W. *Rad. Eff. Def. in Solids*. **2013,** *168*, 902–911.
(2) Yang, J.; Zhao, Y.; Zhu, X. *Appl. Phys. Lett.* **2006,** *88*, 094101.
(3) Vorobyev, A.Y.; Guo, C. *Appl. Phys. Lett*. **2013,** *102*, 074107.

(4) Bonse, J.; Höhm, S.; Rosenfeld, A.; Krüger, J. *Appl. Phys. A.* **2013,** *110*, 547–551.
(5) Derrien, T.J.-Y.; Koter, R.; Krüger, J.; Höhm, S.; Rosenfeld, A.; Bonse, J. *J. Appl. Phys*. **2014,** *116*, 074902.
(6) Sahin, R.; Simsek, E.; Akturk, S. *Appl. Phys. Lett.* **2014,** *104*, 053118.
(7) Gubko, M.A.; Husinsky, W.; Ionin, A.A.; Kudryashov, S.I.; Makarov, S.V.; Nathala, C.R.; Rudenko, A.A.; Seleznev, L.V.; Sinitsyn, D.V.; Treshin, I.V. *Laser Phys. Lett*. **2014,** *11*, 0653011.
(8) Birmbaum, M. *J. Appl. Phys*. **1965,** *36*, 3688.
(9) Sipe, J.E., Young, J.F.; Preston, J.S.; van Driel, H.M. *Phys. Rev. B.* **1983,** *27*, 1141–1154.
(10) Shimotsuma, Y.; Kazansky, P.G.; Qiu, J.; Hirao, K. *Phys. Rev. Lett*. **2003,** *91*, 247405.
(11) Zhao, Q.Z.; Ciobanu, F.; Wang, L.J. *J Appl. Phys*. **2009,** *105*.
(12) Huang, M.; Zhao, F.; Cheng, Y.; Xu, N.; Xu, Z. *ACS Nano*. **2009,** *3*, 4062–4070.
(13) Joannopoulos, J.D.; Meade, R.D.; Winn, J.N. *Photonic Crystals*; Princeton University Press: Princeton, NJ, 1995.
(14) Ropers, C.; Elsaesser, T.; Cerullo, G.; Zavelani-Rossi, M.; Lienau, C. *New J Phys*. **2007,** *9*, 397.
(15) Pomraenke, R.C.R.; Renard, J.; Lienau, C.; Lüer, L.; Polli, D.; Cerullo, G. *Nano Lett*. **2007,** *7*, 998–1002.
(16) Bashir, S.; Rafique, M.S.; Ajami, A.; Husinsky, W.; Kalsoom, U. *Appl. Phys. A.* **2013,** *113*, 673–681.
(17) Nichols, W.T.; Sasaki, T.; Koshizaki, J. *Appl. Phys*. **2006,** *100*, 114913.
(18) Yan, Z.; Bao, D.; Chrisey, B. *Nanotechno*. **2010,** *21*, 145609.
(19) Bashir, S.; Rafique, M.S.; Nathala, C.S.; Husinsky, W. *Appl. Surf. Sci*. **2014,** *290*, 53–58.
(20) Santillán, L.M.J.; Videla, F.A.; Fernández van Raap, D.B.; Schinca, D.C.; Scaffardi, L.B. *J. Appl. Phys*. **2013,** *113*, 134305.
(21) Lang, F.; Mosbacher, M.; Leiderer, P. *Appl. Phys. A.* **2003,** *77*, 117–123.
(22) Kim, J.; Na, S.; Cho, S.; Chang, W.; Whang, K. *Opt. & Laser in Eng*. **2008,** *46*, 306–310.
(23) Albu, C.; Dinescu, A.; Filipescu, M.; Ulmeanu, M.; Zamfirescu, M. *Appl. Surf. Sci*. **2013,** *278*, 347–351.
(24) Yasumaru, N.; Miyazaki, K.; Kiuchi, J. *Appl. Phys. A.* **2005,** *81*, 933–937.
(25) Albu, C.A.; Dinescub, M.; Filipescua, M.; Ulmeanua, M.; Zamfirescua, M. *Appl. Surf. Sci*. **2013,** *278*, 347–351.
(26) Zhu, S.; Lu, Y.F.; Hong, M.H.; Chen, X.X. *J. Appl. Phys*. **2001,** *89*, 2400.
(27) Bonse, J.; Kruger, J. *J. Appl. Phys*. **2010,** *108*, 034903.
(28) Major, A.; Aitchison, J.S.; Smith, P.W.E.; Druon, F.; Georges, P.; Viana, B.; Aka, G.P. *Appl. Phys. B.* **2005,** *80*, 199–201.
(29) Bulgakova, N.M.; Bourakov, I.M. *Appl. Surf. Sci*. **2002,** *197–198*, 41–44.
(30) Vorobyev, A.Y.; Kuzmichev, V.M.; Kokody, N.G.; Kohns, P.; Dai, J.; Guo, C. *Appl. Phys. A.* **2006,** *82*, 357–362.
(31) Kang, H.W.; Lee, H.; Welch, A.J. *J. Appl. Phys*. **2008,** *103*, 083101.
(32) Hwang, T.Y.; Vorobyev, A.Y.; Guo, C. *Phys. Rev. B.* **2009,** *79*, 085425.
(33) Van Driel, H.M.; Sipe, J.E.; Young, J.F. *Phys. Rev. Lett*. **1982,** *49*, 1955–1958.
(34) Derrien, Y.; Itina, T.E.; Torres, R.; Sarnet, T.; Sentis, M. *J. Appl. Phys*. **2013,** *114*, 083104.
(35) Huynh, T.T.D.; Semmar, N. *Appl. Phys. A.* **2014,** *116*, 1429–1435.
(36) Miyaji, G.; Miyazaki, K. *Opt. Exp*. **2008,** *16*, 16265–16271.
(37) Bashir, S., Rafique, M.S.; Husinsky, W. *Nucl. Inst. & Meth. B.* **2012,** *275*, 1–6.
(38) Das, S.K.; Messaoudi, H.; Debroy, A.; McGlynn, E.; Grunwald, R. *Opt. Mat. Exp*. **2013,** *3*, 1705–1715.
(39) Harilal, S.S.; Bindhu, C.V.; Nampoori, V.P.N.; Vallabhan, C.P.G. *Appl. Spect.* **1998,** *52*, 449–455.
(40) Akram, M.; Bashir, S.; Hayatat, A.; Mahmood, K.; Ahmad, R.; Rahaman, M.K. *Laser & Part. Beams*. **2014,** *32*, 119–128.
(41) Harilal, S.S.; Bindhu, C.V.; Nampoori, V.P.N.; Vallabhan, G. *Appl. Phys. Lett*. **1998,** *72*, 167–169.
(42) Bäuerle, D. *Laser Processing and Chemistry*; Springer-Verlag Berlin: New York, 2000.
(43) Socrates, G. *Infrared and Raman Charteristic Group Frequencies (Tables and Charts), 3rd ed.*; John Wiley and Sons, Ltd.: West Sussex, 2001.
(44) Sipe, J.E.; Young, J.F.; Preston, J.S.; Van Driel, H.M. *Phys. Rev. B.* **1983,** *27*, 1141–1154.
(45) Lee, Y.; Becker, M.F.; Walser, R. *J. Opt. Soc. Am. B.* **1988,** *5*, 648.
(46) Kandyla, M.; Shih, T.; Mazur, E. *Phys. Rev. B.* **2007,** *75*, 1–7. art no. 214107.
(47) Amoruso, S.; Ausanio, G.; Bruzzese, R.; Vitiello, M.; Wang, X. *Phys. Rev. B.* **2005,** *71*, 033406.
(48) Bashir, S.; Rafique, M.S.; Husinsky, W. *Appl. Surf. Sci*. **2009,** *255*, 8372–8376.
(49) Rousse, A.; Rischel, C.; Fourmaux, S.; Uschmann, I.; Sebban, S.; Grillon, G.; Balcou, P.; Forster, E.; Geindre, J.P.; Audebert, P.; Gauthier, J.C.; Hulin, D. *Nature*. **2001,** *410*, 65–67.
(50) Miyasaka, Y.; Hashida, M.; Ikuta, Y.; Otani, K.; Tokita, S.; Sakabe, S. *Phys. Rev. B.* **2012,** *86*, 075431.
(51) Stuart, B.C.; Feit, M.D.; Herman, S.; Rubenchik, A.M.; Shore, B.W.; Perry, M.D. *Phys. Rev. B.* **1996,** *53*, 1749–1761.
(52) Vella, A.; Deconihout, B.; Marrucci, L.; Santamato, E. *Phys. Rev. Lett*. **2007,** *99*, 046103.
(53) Monnereau, O.; Tortet, L.; Grigorescu, C.E.A.; Savastru, D.; Iordanescu, C.R.; Guinneton, F.; Notonier, R.; Tonetto, A.; Zhang, T.; Mihailescu, I.N.; Stanoi, D.; Trodahl, H.J. *J. Optoelect. & Advan. Mat*. **2010,** *12*, 1752–1757.